Transactions of the Indian National Academy of Engineering (2020) 5:475–483
https://doi.org/10.1007/s41403-020-00107-9

ORIGINAL ARTICLE

Scalable Synthesis and Kinetic Studies of Carbon Coated Sodium Titanate: A Promising Ultra-low Voltage Anode for Sodium Ion Battery

P. Laxman Mani Kanta[1,2] · M. Venkatesh[1] · Satyesh Kumar Yadav[2] · Bijoy Kumar Das[1] · R. Gopalan[1]

Received: 28 April 2020 / Accepted: 18 May 2020 / Published online: 29 May 2020

Abstract

The ultra-low voltage anode, $Na_2Ti_3O_7$ (NTO) of high specific capacity (177 mAh/g) suffers from low intrinsic electronic conductivity, leading to poor electrochemical performance. Herein, we report the synthesis of carbon-coated $Na_2Ti_3O_7$ (NTO/C) from indigenously prepared TiO_2; where a low-cost organic precursor, resorcinol is used as a carbon source for the first time. Resorcinol derived carbon is beneficial in two ways: (1) increase in electronic conductivity; and (2) promote sodium ion intercalation being electrochemically active. The structural and morphological characterizations are conducted by X-ray diffraction, Fourier transform infra-red spectroscopy, scanning electron microscopy and transmission electron microscopy techniques, which confirm the formation of phase pure NTO/C with cuboid-shaped morphology. The carbon coating along with cuboid type morphology together show improved electrochemical performance due to the increase in electronic conductivity and sodium ion diffusivity. The NTO/C shows higher reversible charge capacity of 213 (±5) mAh/g with 48% capacity retention against 178 (±5) mAh/g with 24% capacity retention for pristine NTO after 40 cycles. Excellent rate capability is seen for NTO/C; where it shows a stable capacity of 70 (±5) mAh/g at 2.0 C-rate. The novelty of this present work involves large scale synthesis of carbon-coated $Na_2Ti_3O_7$ from indigenously prepared TiO_2 and low-cost resorcinol as a source of carbon with improved electrochemical performance, which can be used as promising intercalation based anode material for sodium-ion batteries.

Keywords Sodium titanates · Carbon coating · Cuboid morphology · Electrochemical performance · Anode · Sodium-ion battery

Introduction

Electrochemical energy storage (EES) systems are the most promising secondary storage devices for various applications. These are found to be highly efficient to store the energy produced from renewable sources (Gur et al. 2018; Deng et al. 2018; Liu et al. 2019). Currently, lithium-ion batteries (LIBs) are the most preferred battery chemistry, being widely used for portable electronics to electric vehicles (EVs) (Kim et al. 2012). However, limited availability of lithium (Li) resources can push up the prices of lithium-based compounds, thereby making the LIBs more expensive. Efforts are being made to find a low-cost EES, particularly for grid energy storage. Sodium based battery chemistry has emerged as a low-cost solution for grid energy storage due to the large abundance of sodium resources on Earth's crust and having similar electrochemical properties to that of lithium; though it suffers from little lower in specific energy (Yabuuchi et al. 2014). The major challenge associated with sodium-ion batteries (SIBs) is the lack of suitable electrode materials; particularly negative electrodes (Kubota and Komaba 2015; Li et al. 2018; Hwang et al. 2017). Design and development of negative electrode materials with high specific energy and power is the key challenge lying ahead for the development of SIBs.

Electronic supplementary material The online version of this article (https://doi.org/10.1007/s41403-020-00107-9) contains supplementary material, which is available to authorized users.

✉ Bijoy Kumar Das
bijoy822000@gmail.com

[1] Centre for Automotive Energy Materials (CAEM), International Advanced Research Centre for Powder Metallurgy and New Materials (ARCI), Chennai, Tamil Nadu 600113, India

[2] Department of Metallurgical and Materials Engineering, Indian Institute of Technology Madras (IITM), Chennai, Tamil Nadu 600036, India

Intercalation-based electrode materials are largely being used in batteries due to their ultra-long cycle life at higher current rates (Nava-Avendaño et al. 2015). However, very few intercalation based electrode materials are being explored for SIBs. $Na_2Ti_3O_7$ (NTO) is the first intercalation based oxide material exhibiting an ultra-low sodium ion intercalation at ~ 0.3 V *vs.* Na/Na^+ with a theoretical capacity of 177 mAh/g (Xia et al. 2018). NTO exhibits layered structure (Fig. 1a) (Source: Materials Project open Database), in which each formulae unit consists of two-dimensional sheets of $(Ti_3O_7)^{2-}$ with edge-sharing TiO_6 octahedral chains arranged in a *zigzag* fashion accommodating Na^+ ions in-between them (Guo et al. 2016). Until now, different synthesis routes have been adopted for preparing NTO such as traditional solid state, hydrothermal, solvothermal, and sol–gel using a wide range of precursors (Rudola et al. 2013; Cech et al. 2017; Wang et al. 2013; Zhang et al. 2014). Irrespective of synthesis routes and precursors, NTO exhibits poor electrochemical performance due to its inherent insulating nature (band gap of ~ 3.07 eV) and the brittleness (Zarrabeitia et al. 2016). The volume change of ~ 5% resulted due to the intercalation of two sodium ions to form $Na_4Ti_3O_7$ phase is sufficient to develop electrode cracking and can lead to poor cycle life (Rudola et al. 2013; Cech et al. 2017; Wang et al. 2013; Zhang et al. 2014; Zarrabeitia et al. 2016). Hence, extensive research is going on to improve the electronic conductivity and to minimize the electrode cracking through surface modification of NTO by conductive coatings (Zarrabeitia et al. 2016; Li et al. 2017; Bhardwaj et al. 2018). Zarrabeitia et al. (2016) reported the capacity fade in NTO due to the presence of a small amount of insulating Na_2CO_3, either formed by the surface corrosion or from the unreacted precursor. Li et al. (2017) synthesized carbon-coated NTO nanotubes, which delivered a high reversible capacity of 142.2 mAh/g for over 100 cycles at 1 C-rate. Bhardwaj et al. (2018) reported that the continuous formation of passivation film due to side reactions with the electrolyte is the main reason for capacity degradation. They addressed this issue through uniform wrapping of NTO particles with MWCNT's, which showed better cyclic stability and rate capability. The particle size and morphology of NTO also have a great impact on the electrochemical performance of NTO (Rudola et al. 2013; Cech et al. 2017; Wang et al. 2013; Zhang et al. 2014). Rudola et al. (2013) synthesized the micron-sized NTO particles (~ 1.9 µm) with rod-shaped morphology through the solid-state method, which showed a capacity of 177 mAh/g at 0.1 C rate. Pan et al. (2013) showed a reversible capacity of 188 mAh/g for micron-sized NTO particles at 0.1 C-rate using an optimized electrolyte of 1 M NaFSI in PC and sodium alginate binder, respectively. Wang et al. (2013) synthesized micro-spherical NTO material consisting of tiny nanotubes, which showed a capacity of 108 mAh/g over 100 cycles at a current density of 354 mA/g. The synthesized nanotubes exhibited good cycle life and rate performance because of the increased surface area. Though many attempts were made to improve

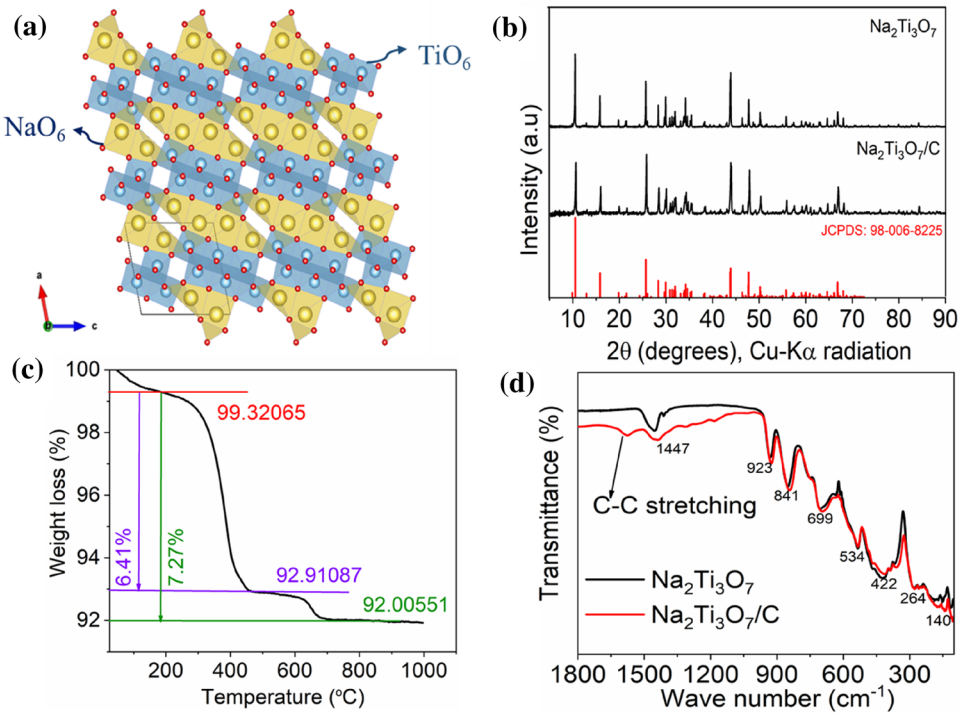

Fig. 1 **a** Crystal structure of $Na_2Ti_3O_7$ showing NaO_6 and TiO_6 octahedra (Source: Materials Project Open Database). **b** X-ray diffraction (XRD) patterns of $Na_2Ti_3O_7$ and $Na_2Ti_3O_7$/C. **c** Thermo gravimetric (TG) analysis plot of $Na_2Ti_3O_7$/C carried out under air atmosphere showing weight loss due to carbon oxidation. **d** FT-IR spectra of $Na_2Ti_3O_7$ and $Na_2Ti_3O_7$/C

the cyclic stability, there is still a great need to improve the performance of NTO in terms of high specific capacity and long cyclic stability.

Herein, we report the synthesis of NTO of large scale using the modified solid-state route, where indigenously prepared anatase-TiO_2 and commercial Na_2CO_3 were used as precursors. Ex-situ carbon coating was carried out using a low-cost resorcinol as a carbon precursor to improve the electronic conductivity. To the best of our knowledge, TiO_2 prepared by flame-spay-pyrolysis (FSP) and resorcinol as source for carbon are used for the first time. Structural and morphological studies reveal the formation of phase pure NTO with cuboid-shaped morphology. Carbon coated NTO has shown higher specific capacity and better capacity retention compared to that of pristine NTO. A high reversible charge specific capacity of ~ 213 (±5) mAh/g has been seen with a capacity retention of 48% at the end of 40 cycles against 178 mAh/g with a capacity retention of 24% for pristine NTO. Excellent rate performance has been recorded for NTO/C even at 2.0 C-rate. The reason for improved electrochemical performance has been explained as the increase in sodium diffusion coefficient (D_{Na+}) and lowering in charge transfer resistance evident from cyclic voltammetry (CV) and electrochemical impedance spectroscopy (EIS) studies, respectively. The improved sodium-ion storage and high rate performance after carbon coating make it as a promising anode material for sodium-ion battery.

Materials and Methods

Material Synthesis

To prepare $Na_2Ti_3O_7$ (hereafter, NTO) in large scale, conventional solid-state synthesis route has been adopted using cheaper precursors such as sodium carbonate (Na_2CO_3, Merck, 99.9%) and indigenously prepared anatase TiO_2 by flame-spray pyrolysis. Initially, Na_2CO_3 and TiO_2 at 1:3 mol ratio (with 5 wt% excess of Na_2CO_3) were mixed thoroughly using a Retsch ball milling unit at 100 rpm for 1 h; followed by calcination of the mixture at 800 °C for 15 h in ambient air atmosphere. The obtained product was subjected to further grinding and reheating at 800 °C for 15 h under air atmosphere to ensure the formation of pure $Na_2Ti_3O_7$ phase. For ex-situ carbon coating, the synthesized NTO was mixed with 10 wt% of resorcinol ($C_6H_6O_2$, Merck, 99%) and the mixture was heated at 500 °C for 4 h under the flowing argon gas in a tubular furnace. The obtained $Na_2Ti_3O_7$ (hereafter, NTO) and carbon-coated $Na_2Ti_3O_7$ (hereafter, NTO/C) were subjected to structural and electrochemical characterization.

Structural Characterization

The wide-angle powder X-ray diffraction (XRD) was carried out to determine the formation of phase pure and crystal structure of NTO and NTO/C using Rigaku smart lab X-ray diffractrometer equipped with Cu-Kα radiation in the 2θ range of 5°–90° at a scan rate of 1°/min. Morphology and elemental compositions were determined by field-emission scanning electron microscopy (FE-SEM) and energy dispersive spectroscopy (EDS) using Carl Zeiss Merlin's field emission scanning electron microscope at an accelerating voltage of 10 kV. Transmission electron microscopy (TEM) was further used to determine the morphology and carbon coating on NTO particles using Technai G2 transmission electron microscope, having lanthanum hexaboride (LaB_6) filament at 200 kV electron beam. The infrared (IR) spectra of pristine NTO and NTO/C were recorded using Fourier transform infrared (FT-IR) spectrometer (Bruker VERTEX 70v) in a scan range of 50–1800 cm^{-1} under the reflectance mode. The amount of carbon present in the NTO/C was determined using thermogravimetric (TG) analyser (Netzsch STA449 F1 Zupiter) at a heating rate of 10 °C/min in air atmosphere.

Electrochemical Characterization

For electrode preparation, a viscous slurry was prepared by thorough mixing of electrode active material (here NTO and NTO/C), conductive carbon black (Super P) and binder (PVDF, Polyvinylidene flouride) in a weight ratio of 75:20:5; where *N*-methyl-2-pyrrolidone (NMP) was used as a solvent. The slurry was coated onto an etched copper current collector (electronic grade, Targray, 10 μm thick) using a doctor blade. The coated electrode was dried in a vacuum oven (Binder GmBH) at 80 °C for 24 h followed by calendaring at a pressure of 3000 psi. The dried electrodes were taken inside an argon-filled glove box, where H_2O and O_2 levels were maintained < 0.1 ppm. 2032 type coin cells were fabricated using the electrode with diameter, $\Phi \sim 15$ mm; where glass microfiber filter (Whatmann GF/D) of diameter $\Phi \sim 19$ mm was used as a separator. Sodium metal (sigma Aldrich, 99.99%) was used as a counter/reference electrode; whereas indigenously prepared 1 M $NaClO_4$ in EC:PC (1:1 by vol%) was used as the electrolyte. Cyclic voltammetry (CV) and galvanostatic charge/discharge cycling with potential limitation (GCPL) were carried out on coin-type cells using Biologic battery tester (BCS-810). Electrochemical impedance spectroscopic (EIS) studies were conducted on pristine NTO and NTO/C-based coin cells using AMETEK PARSTAT MC electrochemical work station at an applied ac voltage of 10 mV in the frequency range of 1 mHz–10 mHz.

Results and Discussion

The XRD patterns of pristine $Na_2Ti_3O_7$ (hereafter, NTO) and carbon-coated $Na_2Ti_3O_7$ (hereafter, NTO/C) are shown in Fig. 1b. The formation of phase pure NTO without any noticeable impurities has been seen after the calcination at 800 °C for 30 h in ambient air atmosphere. During the first step of calcination at 800 °C for 15 h, the formation of mixed phase of both NTO and $Na_2Ti_6O_{13}$ were seen (Supplementary Fig. S1). The formation of Ti-rich secondary phase, $Na_2Ti_6O_{13}$ is due to the lower Gibbs free energy of formation (− 5915.4 kJ/mol) compared to NTO (− 3288.2 kJ/mol) (Holzinger et al. 2003). However, the presence of $Na_2Ti_6O_{13}$ phase has a negative impact on the electrochemical performance of NTO as evident from the reported literature (Cech et al. 2017). Hence, heating under the same temperature for an additional 15 h was carried out to eliminate the $Na_2Ti_6O_{13}$ phase and to achieve phase pure NTO (Fig. 1b). No secondary phase has been detected after ex-situ carbon coating at 500 °C in argon atmosphere (Fig. 1b). The observed XRD patterns of both NTO and NTO/C shown in Fig. 1b are well matched with the reference data (JCPDS: 98-006-8225), belonging to the monoclinic crystal structure with a space group of $P2_1/m$. The crystal framework of NTO as shown in Fig. 1a is formed by TiO_6 octahedra connected by edges and stacked to form a layered structure; where Na^+-ions occupy two crystallographic sites, one with ninefold coordination and other with sevenfold coordination between the slabs of TiO_6 octahedra. These Na^+-ions diffuse through the channels during charge/discharge process with a low activation energy of 0.186 eV (Pan et al. 2013).

NTO is insulating in nature having bandgap energy in the range of 2.9–3.5 eV as calculated from DFT (Araújo-Filho et al. 2017). To improve the electronic conductivity, we adopted a conductive carbon coating onto the NTO using resorcinol as a source of carbon ($C_6H_6O_2$). Resorcinol, which is mostly used in resins, cosmetics and pharmaceuticals, can easily be decomposed to carbon at very low temperature (≤ 260 °C) (Trivedi et al. 2015; Alcántara et al. 2005). It is known that hard microspherical carbon derived from resorcinol showed promising sodium ion intercalation at low potential and thereby justifying its use as carbon coating to improve the performance by increasing electronic conductivity as well as promoting sodium ion intercalation being electrochemically active at the same electrochemical window of NTO (Alcántara et al. 2005). It may also protect NTO from undesired side reaction with electrolyte and provide additional mechanical strength preventing cracking of electrode during cycling. The decomposition temperature of resorcinol is far lower compared to the NTO synthesis temperature, making it suitable for carbon coating without any structural change in NTO. Carbon coating on NTO has been carried out at 500 °C for 4 h in argon atmosphere to ensure relatively high electronic conductivity of carbon. Thermogravimetric (TG) analysis has been carried on NTO/C as shown in Fig. 1c, to determine the carbon content. The major weight loss of 6.41% seen around 300–450 °C is due to the loss of carbon in the form of CO or CO_2. In addition, negligible weight loss of 0.86% around 450–700 °C is also noticed, followed by a stable phase up to 1000 °C. The minor weight loss around 450–700 °C could be due to the oxidation of unaccessed carbon, which needs to be further studied. The carbon content estimated form TG plot (Fig. 1c) is ~ 7.27 wt%. Figure 1d depicts the FT-IR spectra of pure NTO and NTO/C in the far- and mid-infrared region. The absorption bands seen for both NTO and NTO/C are the same without any noticeable additional bands except the band due to C–C stretching at 1589 cm^{-1}. The absorption spectra consist of nearly 6 major bands and 2 minor bands in the range of 100–1800 cm^{-1}. The most intense IR bands at 422, 534, 699, 841, 923 and 1447 cm^{-1} are possibly due to the O–Ti–O stretching and bending bands of TiO_6 octahedra and the bands at 140 and 264 cm^{-1} are possibly due to O–Na–O stretching and bending bands of NaO_6 octahedra, respectively (Silva et al. 2018).

Figure 2a, b depict the SEM images of pure NTO and NTO/C; where a cuboid-shaped morphology with a wide range of particle sizes of different aspect ratios are seen. In both NTO and NTO/C, particles grew to different lengths in the range of 2–4 µm. Energy dispersive spectroscopic (EDS) analysis reveals the presence of all the elements at a stoichiometric atomic/weight ratio (Fig. 2d). The morphology of NTO/C was further studied by TEM analysis and the image of a single NTO/C particle is shown in Fig. 2c. The cuboid-shaped particle morphology of ~ 1400 nm in length and ~ 600 nm in width maintaining an aspect ratio of 2.33 is seen. Nearly uniform and thick carbon coating of ~ 10 nm has been observed from the TEM image (Fig. 2c).

Cyclic voltammetry (CV) studies on both pristine NTO and NTO/C was carried out against Na-metal at 0.1 mV/s in the voltage window of 0.01–2.5 V vs. Na/Na^+, to evaluate the electrochemical behaviour. The CV plots of NTO and NTO/C for 1st, 2nd and 5th cycles are shown for clarity in Fig. 3a, b, respectively. During the first cathodic (reduction) scan (Fig. 3a), pristine NTO shows a continuous fall of cell potential up to 0.8 V, followed by two intense peaks centred at ~ 0.41 and ~ 0.12 V, which correspond to the irreversible formation of a surface film on NTO due to the electrolyte decomposition and sodium intercalation to $Na_2Ti_3O_7$ structure to form $Na_{2+x}Ti_3O_7$ ($x \leq 2$), respectively (Rudola et al. 2013; Cech et al. 2017; Wang et al. 2013; Zhang et al. 2014; Muñoz-Márquez et al. 2015). During the first anodic (oxidation) scan, it shows an intense peak centred at ~ 0.32 V;

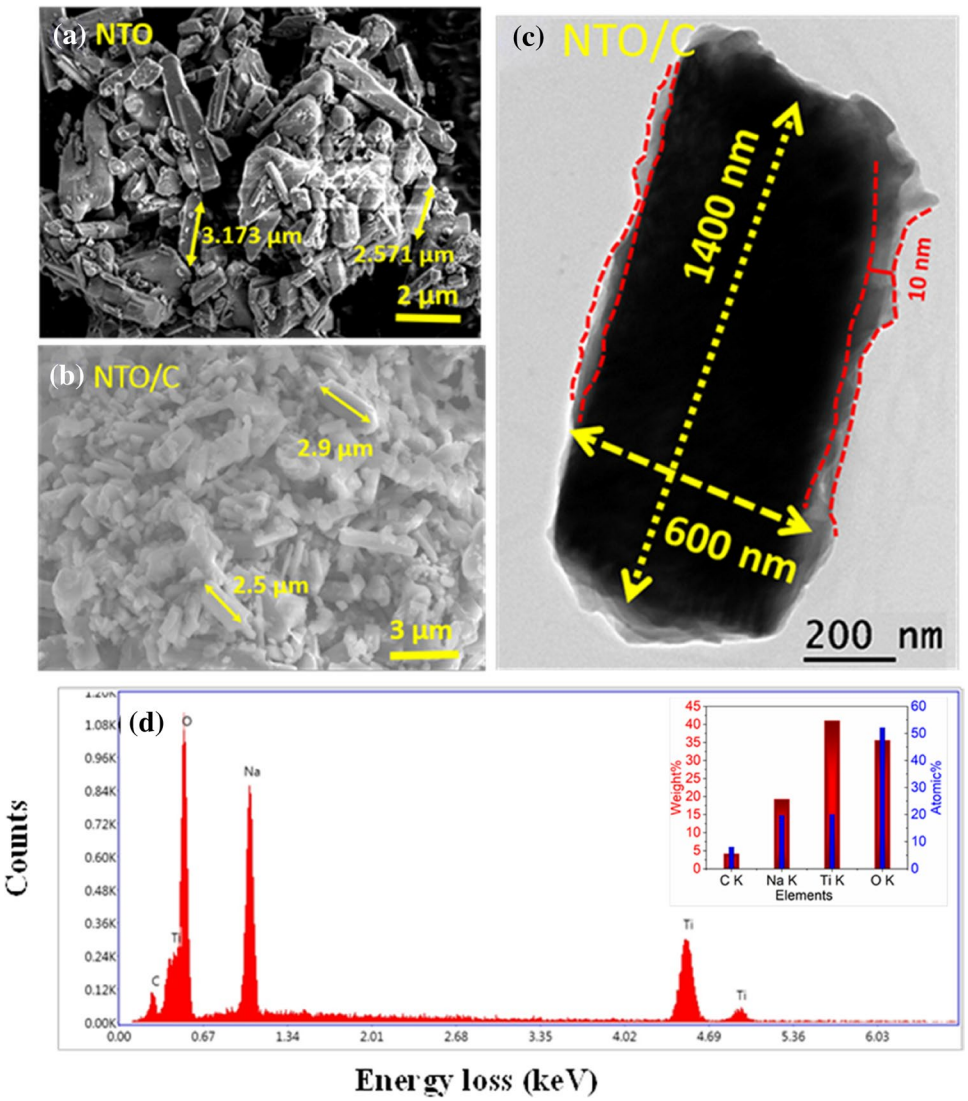

Fig. 2 SEM images of **a** $Na_2Ti_3O_7$ and **b** $Na_2Ti_3O_7$/C. **c** TEM image of $Na_2Ti_3O_7$/C showing carbon coating. **d** EDAX plot of $Na_2Ti_3O_7$/C (inset is the weight and atomic% of different elements present in the $Na_2Ti_3O_7$)

followed by a shoulder peak at ~ 0.48 V, which reveal the sodium extraction from NTO in two-steps (Fig. 3a). The reduction peak noticed at ~ 0.41 V during first cathodic scan disappears completely in the second and 5th cathodic scan suggesting irreversibility in the formation of the surface film; whereas the peak noticed at ~ 0.12 V remained unchanged, confirming similar sodium ion intercalation mechanism. The second anodic profile is similar to that of the first anodic scan showing no change/shift of oxidation peak. Oxidation peak shifting to higher voltage is seen during 5th anodic scan, possibly due to the surface modification of NTO. Excellent reversibility of sodium ion intercalation/de-intercalation into/from NTO has been evident from similar redox potential noticed during 2nd and 5th cycles. The area under the CV curves for 1st-to-5th cycles decreases with an increase in cycle number, indicating capacity degradation. The CV plots for NTO/C is quite interesting and the reduction peak at ~ 0.41 V during first cathodic scan associated to the electrolyte decomposition and formation of a surface film on pure NTO is absent in case of NTO/C (Fig. 3b). This is possibly due to carbon coating onto NTO, which minimizes the exposure of NTO surface to the electrolyte. The redox peaks due to sodium ion intercalation/de-intercalation are at the same voltage; while no shoulder peak is observed during anodic scan indicating sodium ion extraction in single-step unlike two-step de-intercalation process observed in pure NTO. The single-step intercalation can be attributed to the increase in electronic conductivity after carbon coating. The CV plots overlap each other from 1st to 5th cycles indicating excellent reversibility and better capacity retention compared to that of pure NTO.

The electrochemical performance of NTO and NTO/C was further studied by galvanostatic discharge/charge cycling against Na-metal at 0.1 C-rate (1 C = 177 mA/g) in the voltage window of 0.01–2.5 V *vs.* Na/Na^+ and the characteristic charge–discharge profiles for 1st cycle are

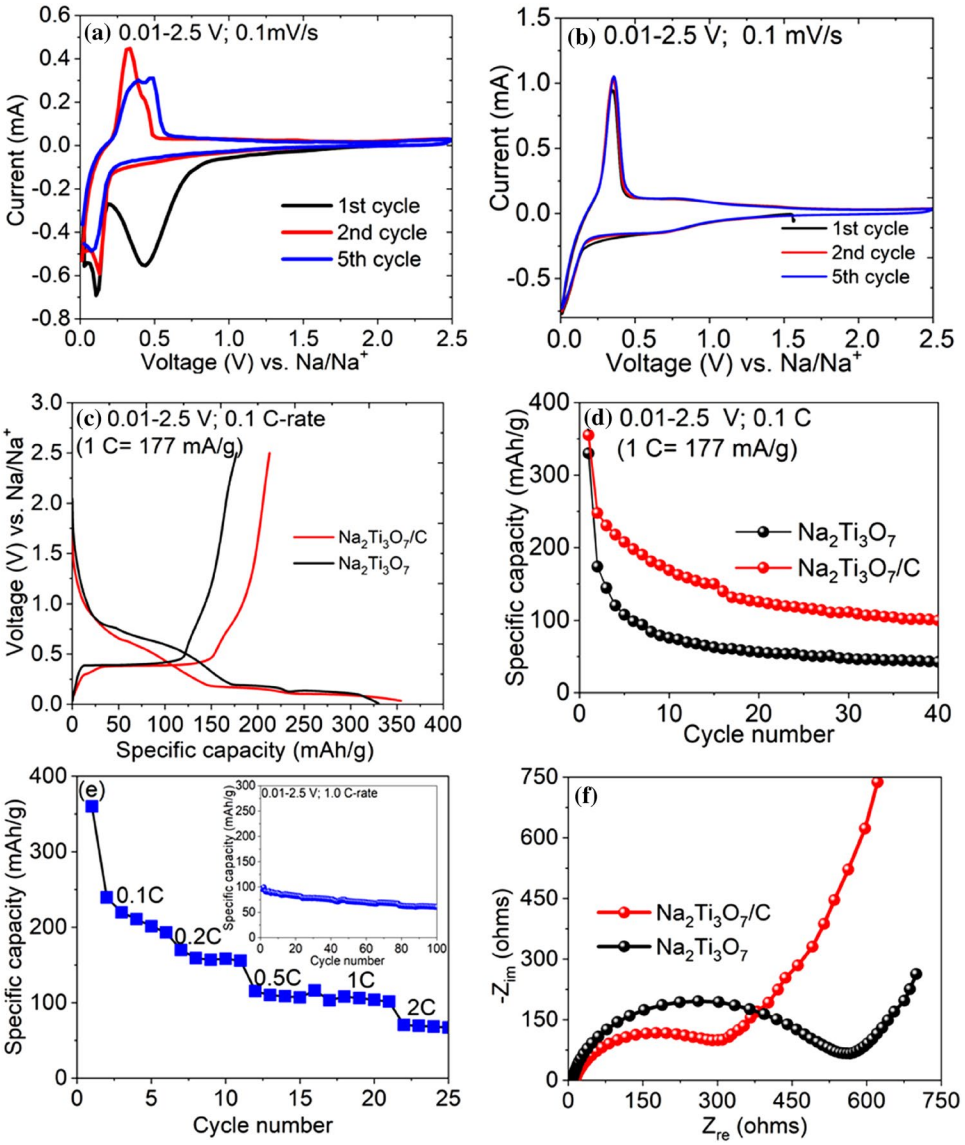

Fig. 3 Cyclic voltammograms of **a** $Na_2Ti_3O_7$ and **b** $Na_2Ti_3O_7$/C for 1st, 2nd and 5th cycle cycled at 0.1 mV/s in the voltage window of 0.01–2.5 V vs. Na/Na^+. **c** 1st cycle galvanostatic discharge/charge plots of $Na_2Ti_3O_7$ and $Na_2Ti_3O_7$/C cycled at 0.1 C-rate in the voltage window of 0.01–2.5 V vs. Na/Na^+. **d** Specific capacity vs. cycle number plots of $Na_2Ti_3O_7$ and $Na_2Ti_3O_7$/C up to 40 cycles cycled at 0.1 C-rate in the voltage window of 0.01–2.5 V vs. Na/Na^+. **e** Specific capacity vs. cycle number plots of $Na_2Ti_3O_7$/C cycled at different C-rates in the voltage window of 0.01–2.5 V vs. Na/Na^+ (inset is the specific capacity vs. cycle number at 1.0 C rate). **f** Nyquist plots of $Na_2Ti_3O_7$ and $Na_2Ti_3O_7$/C recorded at OCV in the frequency range of 1 mHz–10 mHz

shown in Fig. 3c. The specific capacity was calculated w.r.t. the total weight of the NTO and NTO/C active electrode. During the first cycle, NTO delivers a high discharge and charge specific capacities of 330 (±5) and 178 (±5) mAh/g, respectively, with low coulombic efficiency of 54%. Similar cycling profile is seen for NTO/C, where it shows first discharge and charge specific capacity of 355 (±5) and 213 (±5) mAh/g with little higher columbic efficiency of 60%. It can be seen that the first discharge capacity of both NTO and NTO/C is higher than the theoretical specific capacity, which is due to the consumption of additional sodium ions due to the decomposition of electrolyte when cycled to a lower voltage, leading to the formation of the surface film (solid electrolyte interface, SEI layer) on NTO (Muñoz-Márquez et al. 2015). The observed first charge specific capacity for NTO/C is much higher than that of NTO and even higher than the theoretical value. The reason for higher specific capacity can be attributed to the presence of carbon coating which increases the electronic conductivity of the electrode material and thereby increases the utilization of active material. The observed capacity higher than theoretical capacity is possibly due to the additional interfacial storage of sodium ion, which needs further study to understand.

Figure 3d depicts specific capacity vs. cycle number plots for NTO and NTO/C at 0.1 C-rate (1 C = 177 mA/g) for 40 cycles in the voltage window of 0.01–2.5 V vs. Na/Na^+. Both NTO and NTO/C show high first cycle discharge specific capacities of 330 (±5) and 355 (±5) mAh/g with coulombic efficiency as low as 54 and 60%, respectively. When cycled further, slow capacity degradation is seen up to 40 cycles. The NTO/C shows higher specific capacity with better capacity retention compared to pure NTO due to the presence of the carbon coating which increases the electronic conductivity of active electrode material and hence,

promoting the sodium ion intercalation/de-intercalation. In addition, reduction in the formation of surface film onto NTO due to electrolyte decomposition could be another reason for improved electrochemical performance in NTO/C (Fig. 3f). The increase in electronic conductivity in active electrode after carbon coating is evident from the Nyquist plot (Fig. 3f), which shows lower resistance due to surface film and charge transfer in NTO/C compared to pure NTO. It can also be seen that the capacitance due to the formation of a double layer is also lowered after carbon coating, which could be due to lesser polarization of electrolyte at the electrode/electrolyte interface. The lower resistance due to surface film and charge transfer as well as lower in capacitance might have favored the sodium storage leading to higher specific capacity and better capacity retention. The NTO/C delivers a specific capacity of 102 (±5) mAh/g with a capacity retention of 48% after 40 cycles (based on first cycle reversible capacity); whereas NTO delivers only 43 mAh/g with a capacity retention of 24%. The rate performance of NTO/C at different current rates (C-rates) up to 25 cycles was performed to understand the tolerance of the electrode material to high C-rates (Fig. 3e) (Only discharge capacities are given). It shows high reversible specific capacities of 239, 168, 113, 102 and 70 mAh/g at 0.1, 0.2, 0.5, 1.0 and 2.0 C-rates, respectively. The gradual capacity fade is more prevalent at lower C-rates compared to higher C-rates due to longer exposure of active material to the electrolyte, which results in the formation of irreversible products responsible for the capacity fade. The high and stable specific capacities observed at higher C-rates indicate the high tolerance of the electrode material and confirm its suitability for high power applications. To evaluate the suitability of the electrode material for long term cycling, the charge/discharge cycling of NTO/C was carried out for 100 cycles at 1.0 C-rate and the plot is given as inset in Fig. 3e. It can be seen that a high initial reversible capacity of 102 (±5) mAh/g is seen with a capacity retention of 63% at the end of 100 cycles. Further optimization is under progress to synthesize nano-size NTO with uniform carbon coating of a lesser thickness (~3 to 5 nm) to improve the cyclic stability.

The CV measurements were conducted on NTO/C and NTO at different scan rates to understand the sodium ion kinetics and to evaluate the sodium ion diffusion coefficient (D_{Na+}) (Fukuzumi et al. 2016). The CV plots for NTO/C and NTO at selected scan rates (scan rates are given in the plots) from 0.1 to 20 mV/s are shown in Fig. 4a, c, respectively. It can be seen that with an increase in scan rates, the anodic (oxidation) and cathodic

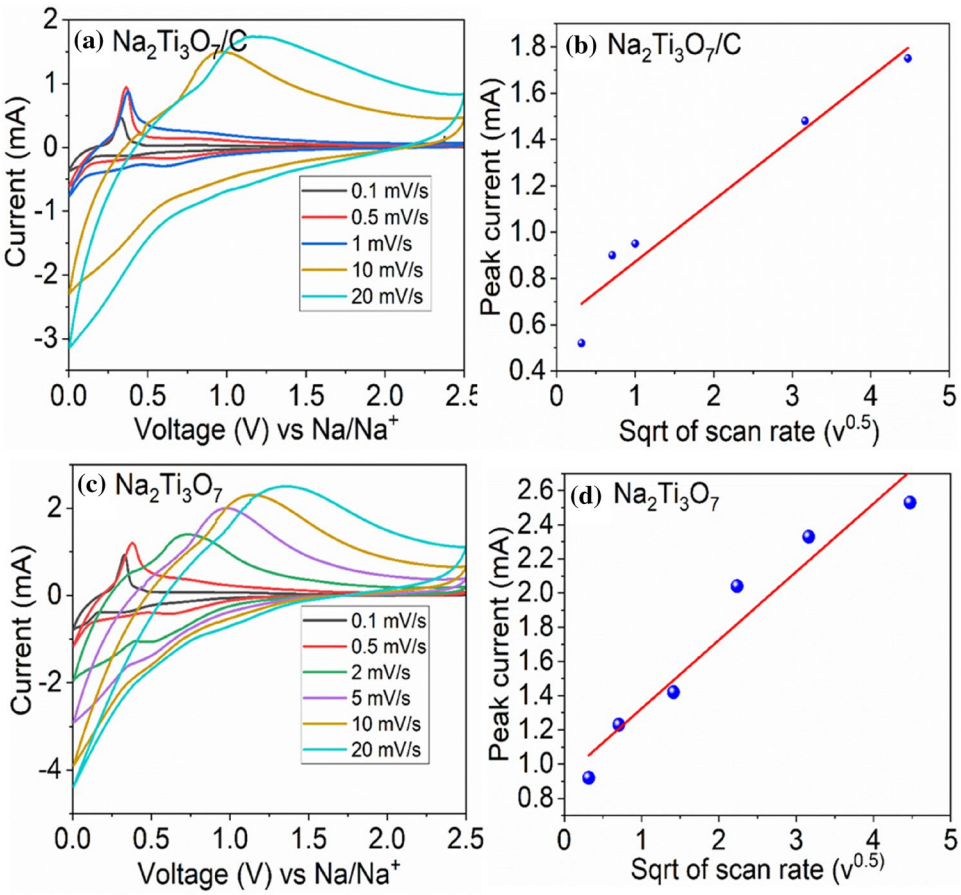

Fig. 4 Cyclic voltammograms at different scan rates in the voltage window of 0.01–2.5 V vs. Na/Na^+ **a** $Na_2Ti_3O_7/C$ and **c** $Na_2Ti_3O_7$. Peak current vs. square root of scan rate plots for **b** $Na_2Ti_3O_7/C$ and **d** $Na_2Ti_3O_7$

Table 1 Electrochemical impedance spectroscopy (EIS) data and Na-ion diffusion coefficient (D_{Na+}) of $Na_2Ti_3O_7$ and $Na_2Ti_3O_7$/C calculated from cyclic voltammetry (CV)

Systems	Electrochemical impedance spectroscopy (EIS) data		Na-ion diffusion coefficient (D_{Na+}) ($\times 10^{-12}$ cm^2/s)
	Rs (Ω)	R(sf + ct) (Ω)	
$Na_2Ti_3O_7$	12.5	547	0.2–0.44
$Na_2Ti_3O_7$/C	6.5	295	3.0–5.8

(reduction) peaks current increase during both the processes for NTO/C and NTO. The gradual shifting of anodic peaks current has been noticed to a higher potential for NTO possibly due to the kinetic limitation by virtue of its intrinsic insulating nature (Fig. 4c). However, such shifting is drastically minimized at least up to 1.0 mV/s after carbon coating due to the increase in conductivity (Fig. 4a). The difference between cathodic and anodic peak current, which gradually increase with the increase in scan rates, confirms different kinetics of sodium ion intercalation/de-intercalation during discharge and charge process. Figure 4b, d show the plots of anodic peaks current (I_p) against the square root of scan rates for NTO/C and NTO. Only anodic peaks current are taken into consideration as no definite cathodic peaks are seen at higher scan rates for both NTO/C and NTO. Observed anodic peaks current follow a linear relationship with the square root of the scan rates, confirming sodium ion intercalation/de-intercalation process through solid-state diffusion (Fukuzumi et al. 2016). Further, sodium ion diffusion co-efficient (D_{Na+}) were calculated from Fig. 4, using Randles–Sevcik equation (Eq. 1) as given below along with experimental parameters.

$$I_p = PD_{Na+}^{1/2} v^{1/2} \quad (1)$$

where P is a constant and calculated from charge transfer number, Faraday's constant (96,486 C mol^{-1}), concentration of sodium ion in moles, surface area of the electrode (cm^2), gas constant (8.314 J mol^{-1} K^{-1}) and absolute temperature (K). The D_{Na+} is the chemical diffusion coefficient (cm^2 s^{-1}) of Na-ion, and v is scan rate (V s^{-1}). The estimated values of D_{Na+} obtained from Eq. (1) are found to be in the range of 2–4.4 $\times 10^{-13}$ cm^2/s for NTO and 3.0–5.8 $\times 10^{-12}$ cm^2/s for NTO/C (Table 1). The D_{Na+} of NTO/C is found to be one order higher than that of NTO due to the increase in conductivity achieved from carbon coating. The observed high and stable specific capacities at higher C-rates for NTO/C can be further co-related to the higher diffusion co-efficient of sodium ions.

Conclusion

In summary, we have synthesized pure $Na_2Ti_3O_7$ (NTO) and carbon-coated $Na_2Ti_3O_7$ (NTO/C) through a solid-state route using indigenously developed TiO_2. A low-cost organic precursor, resorcinol has been used as a carbon source. The pure phase cuboid-shaped NTO with carbon coating of thickness ~ 10 nm has been confirmed from X-ray diffraction (XRD), scanning electron microscopy (SEM) and transmission electron microscopy (TEM) techniques. The cuboid type NTO/C having 2–3 µm in length and 500–600 nm in width has demonstrated superior sodium-ion storage performance compared to pure NTO. The NTO/C has shown much higher reversible charge capacity of 213 (± 5) mAh/g with 48% capacity retention against 178 (± 5) mAh/g with 24% capacity retention after 40 cycles. Excellent rate capability has been seen for NTO/C; where it has shown the a stable capacity of 70 (± 5) mAh/g at 2.0 C-rate. The improvement in electrochemical performance after carbon coating can be ascribed to the synergetic effect of (a) lowering in the resistance due to surface film and charge transfer; (b) high sodium ion diffusivity due to the unique cuboid-shaped microstructure and carbon coating. The large scale synthesis of carbon-coated $Na_2Ti_3O_7$ from indigenously prepared TiO_2 and low-cost resorcinol with improved electrochemical performance makes it as a promising intercalation anode material for sodium-ion batteries.

Acknowledgements The authors would like to acknowledge the financial support from Department of Science and Technology through Technical Research Centre (TRC project: AI/1/65/ARCI/2014) and DST project: DST/TMD/MES/2K17/46, Government of India for the completion of the work. The authors also like to thank Dr. G. Padmanabham, Director, ARCI and Dr. G. Sundararajan, Distinguished Scientist, ARCI for valuable suggestions and continuous support to carry out this work.

Compliance with Ethical Standards

Conflict of interest The authors declare that there are no conflicts of interest.

References

Alcántara R, Lavela P, Ortiz GF, Tirado JL (2005) Carbon microspheres obtained from resorcinol-formaldehyde as high-capacity electrodes for sodium-ion batteries. Electrochem Solid-State Lett 8:A222–A225

Araújo-Filho AA, Silva FL, Righi A, da Silva MB, Silva BP, Caetano EW, Freire VN (2017) Structural, electronic and optical properties of monoclinic $Na_2Ti_3O_7$ from density functional theory calculations: A comparison with XRD and optical absorption measurements. J Solid-State Chem 250:68–74

Bhardwaj HS, Ramireddy T, Pradeep A, Jangid MK, Srihari V, Poswal HK, Mukhopadhyay A (2018) Understanding the cyclic (in) stability and the effects of presence of a stable conducting network on the electrochemical performances of $Na_2Ti_3O_7$. ChemElectroChem 5:1219–1229

Cech O, Castkova K, Chladil L, Dohnal P, Cudek P, Libich J, Vanysek P (2017) Synthesis and characterization of $Na_2Ti_6O_{13}$ and $Na_2Ti_6O_{13}$/$Na_2Ti_3O_7$ sodium titanates with nanorod-like structure as negative electrode materials for sodium-ion batteries. J Energy Storage 14:391–398

Deng J, Luo WB, Chou SL, Liu HK, Dou SX (2018) Sodium-ion batteries: from academic research to practical commercialization. Adv Energy Mater 8:1701428

Fukuzumi Y, Kobayashi W, Moritomo Y (2016) Size dependent ion diffusion in $Na_2Ti_3O_7$ and $Na_2Ti_6O_{13}$. J Adv Nanomater 1:39

Guo S, Yi J, Sun Y, Zhou H (2016) Recent advances in titanium-based electrode materials for stationary sodium-ion batteries. Energy Environ Sci 9:2978–3006

Gür TM (2018) Review of electrical energy storage technologies, materials and systems: challenges and prospects for large-scale grid storage. Energy Environ Sci 11:2696–2767

Holzinger M, Benisek A, Schnelle W, Gmelin E, Maier J, Sitte W (2003) Thermodynamic properties of $Na_2Ti_6O_{13}$ and $Na_2Ti_3O_7$: electrochemical and calorimetric determination. J Chem Thermodyn 35(9):1469–1487

Hwang JY, Myung ST, Sun YK (2017) Sodium-ion batteries: present and future. Chem Soc Rev 46:3529–3614

Kim SW, Seo DH, Ma X, Ceder G, Kang K (2012) Electrode materials for rechargeable sodium-ion batteries: potential alternatives to current lithium-ion batteries. Adv Energy Mater 2:710–721

Kubota K, Komaba S (2015) Practical issues and future perspective for Na-ion batteries. J Electrochem Soc 162:A2538–A2550

Li M, Xiao X, Fan X, Huang X, Liu Y, Chen L (2017) Carbon coated sodium-titanate nanotube as an advanced intercalation anode material for sodium-ion batteries. J Alloys Compd 712:365–372

Li L, Zheng Y, Zhang S, Yang J, Shao Z, Guo Z (2018) Recent progress on sodium ion batteries: potential high-performance anodes. Energy Environ Sci 11:2310–2340

Liu T, Zhang Y, Jiang Z, Zeng X, Ji J, Li Z, Gao X, Sun M, Lin Z, Ling M, Zheng J (2019) Exploring competitive features of stationary sodium ion batteries for electrochemical energy storage. Energy Environ Sci 12:1512–1533

Muñoz-Márquez MA, Zarrabeitia M, Castillo-Martínez E, Eguía-Barrio A, Rojo T, Casas-Cabanas M (2015) Composition and evolution of the solid-electrolyte interphase in $Na_2Ti_3O_7$ electrodes for Na-ion batteries: XPS and Auger parameter analysis. ACS Appl Mater Interfaces 7:7801–7808

Nava-Avendaño J, Morales-García A, Ponrouch A, Rousse G, Frontera C, Senguttuvan P, Tarascon JM, Arroyo-de Dompablo ME, Palacín MR (2015) Taking steps forward in understanding the electrochemical behavior of $Na_2Ti_3O_7$. J Mater Chem A 3:22280–22286

Pan H, Lu X, Yu X, Hu YS, Li H, Yang XQ, Chen L (2013) Sodium storage and transport properties in layered $Na_2Ti_3O_7$ for room-temperature sodium-ion batteries. Adv Energy Mater 3:1186–1194

Rudola A, Saravanan K, Mason CW, Balaya P (2013) $Na_2Ti_3O_7$: an intercalation based anode for sodium-ion battery applications. J Mater Chem 1:2653–2662

Silva FLRE, Filho AAA, da Silva MB, Balzuweit K, Bantignies JL, Caetano EWS, Righi A (2018) Polarized Raman, FTIR, and DFT study of Na2Ti3O7 microcrystals. J Raman Spectroscopy 49:538–548

Trivedi M, Branton A, Trivedi D, Nayak G, Singh R, Jana S (2015) Characterisation of physical, spectral and thermal properties of biofield treated resorcinol. Org Chem Curr Res 4:3

Wang W, Yu C, Lin Z, Hou J, Zhu H, Jiao S (2013) Microspheric $Na_2Ti_3O_7$ consisting of tiny nanotubes: An anode material for sodium-ion batteries with ultrafast charge–discharge rates. Nanoscale 5:594–599

Xia J, Zhao H, Pang WK, Yin Z, Zhou B, He G, Guo Z, Du Y (2018) Lanthanide doping induced electrochemical enhancement of $Na_2Ti_3O_7$ anodes for sodium-ion batteries. Chem Sci 9:3421–3425

Yabuuchi N, Kubota K, Dahbi M, Komaba S (2014) Research development on sodium-ion batteries. Chem Rev 114:11636–11682

Zarrabeitia M, Castillo-Martínez E, Del Amo JM, Eguía-Barrio A, Muñoz-Márquez MÁ, Rojo T, Casas-Cabanas M (2016) Identification of the critical synthesis parameters for enhanced cycling stability of Na-ion anode material $Na_2Ti_3O_7$. Acta Mater 104:125–130

Zhang Y, Guo L, Yang S (2014) Three-dimensional spider-web architecture assembled from $Na_2Ti_3O_7$ nanotubes as a high performance anode for a sodium-ion battery. Chem Comm 50:14029–14032